Electronic Supplementary Information for

Nanopatterned Polymer Brushes as Switchable Bioactive Interfaces

Qian Yu,[a#] Phanindhar Shivapooja,[a#] Leah M. Johnson,[a] Getachew Tizazu,[a] Graham J. Leggett,[d] and Gabriel P. López[abc]*

[a] Department of Biomedical Engineering, Duke University, Durham, NC, 27708, USA.

[b] Department of Mechanical Engineering and Materials Science, Duke University, Durham, NC, 27708, USA.

[c] NSF Research Triangle Materials Research Science & Engineering Center, Duke University, Durham, NC, 27708, USA.

[d] Department of Chemistry, University of Sheffield, Brook Hill, Sheffield, S3 7HF, UK

[#]These authors contributed equally to this work.

1. EXPERIMENTAL SECTION

1.1 Materials

N-isopropylacrylamide (NIPAAm), Cu(II)Br (98% pure), 1,1,4,7,7--pentamethyldiethylenetriamine (PMDETA, 99% pure) and ascorbic acid (reagent grade, 20-200 mesh) (Sigma-Aldrich) were used as received. The ATRP initiator, (3-trimethoxysilyl) propyl 2-bromo 2-methylpropionate (Gelest), was stored under dry conditions until used. Silicon wafers and coverslips were purchased from University Wafer and VWR, respectively.

Biotinylated bovine serum albumin (BSA-biotin) was obtained from Vector Laboratories. Alexa Fluor®488 conjugated-BSA (BSA-Fluor), Alexa Fluor®488 conjugated-streptavidin (SA-Fluor), biotin conjugated yellow-green fluorescent (505/515) nanoparticles (40 nm, 1% solids) (Biotin-NPs) and streptavidin conjugated yellow-green fluorescent (505/515) nanoparticles (40 nm, 0.5% solids) (SA-NPs) were obtained from Invitrogen and stored at 4°C until use. (4-(2-Hydroxyethyl) piperazine-1-ylethanesulphonic acid) (HEPES) and phosphate-buffered saline (PBS) were obtained from BDH Chemicals. NIH-3T3 fibroblast cells were obtained from Duke University Cell Culture Facility.

1.2 Preparation of SAMs of ATRP Initiators

The silicon wafers (2cm x 1cm) and cover slips (2cm x 1cm) were cleaned in "Piranha" solution (H_2SO_4:H_2O_2=7:3(v/v) (**Caution: piranha solution reacts violently with organic materials and should be handled carefully!**) to remove the organic residues from the surface. The wafers were subsequently rinsed with an abundance of ultrapure water and dried under a nitrogen stream. The cleaned samples were immersed in 10 mL of anhydrous toluene containing the ATRP initiator terminated silane (2 vol.%) at room temperature for 24 h to generate brominated surfaces. These surfaces were rinsed thoroughly with toluene and dried under a nitrogen flow.

1.3 Surface Patterning

1.3.1 Photo-oxidation and Patterning of SAMs

Interferometric lithography (IL) was performed using a two-beam interference system (Lloyd's mirror set-up) as reported previously.[1] Nanopatterns of ATRP initiator were fabricated by exposing ATRP initiator immobilized SAMs to a diode-pumped, frequency-doubled Nd: vanadate laser (Coherent, Verdi-V5) with a wavelength of 266 nm. Some nanopatterned surfaces were further exposed to the laser beam through a transmission electron microscope grid containing micron-scale features that resulted in a sample with both micro and nano patterned SAMs of ATRP initiators as shown in **Scheme S1**. This dual-exposure technique permits convenient comparison of nanopatterned and non-patterned areas on the same sample.

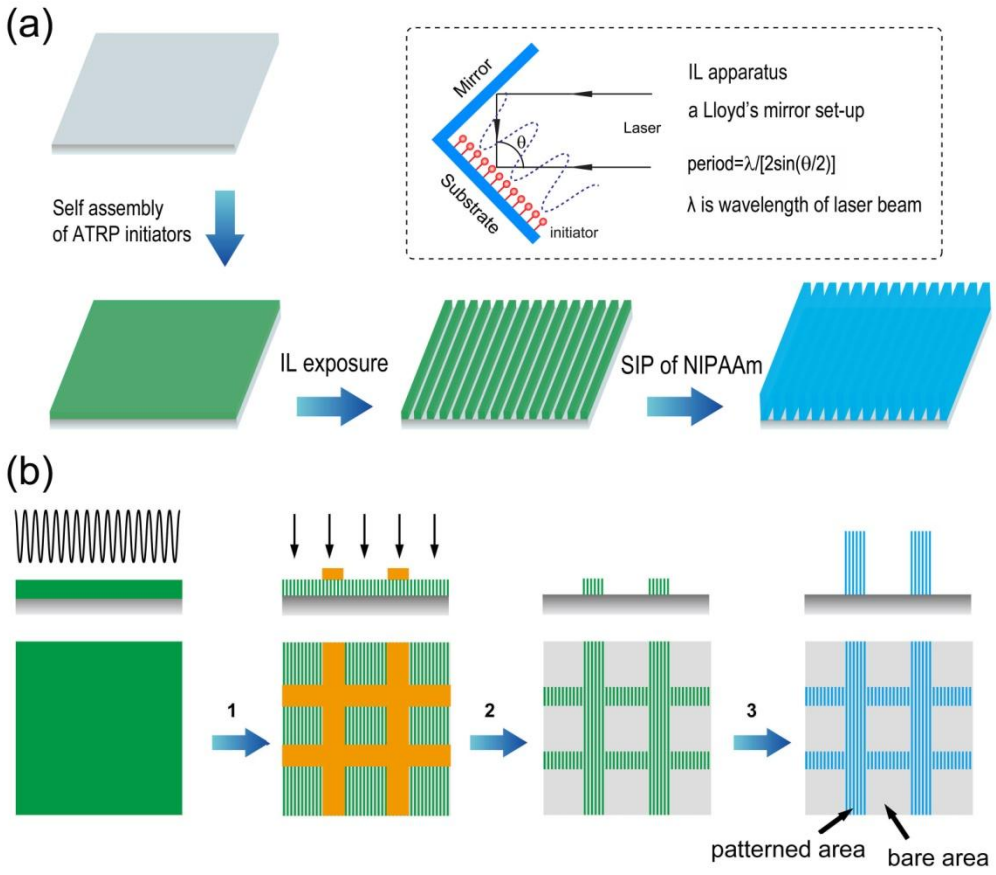

Scheme S1 (a) Procedure of preparation of nanopatterned PNIPAAm brushes. (b) Preparation of micro- and nanopatterned PNIPAAm brushes: (1) IL exposure on SAMs of ATRP initiators; (2) laser exposure through a transmission electron microscope grid mask of a surface containing nanopatterned SAMs of ATRP initiators; (3) surface-initiated polymerization of NIPAAm.

1.3.2 Preparation of PNIPAAm Brushes

PNIPAAm polymer brushes were grafted from the patterned SAMs of ATRP initiators via activators regenerated by electron transfer-atom transfer radical polymerization (ARGET-ATRP). Samples were immersed into a solution containing 14 mL methanol, 14 mL H_2O, 2.5 g NIPAAm, 3.15 mg $CuBr_2$, 34.5 mg ascorbic acid and 19.6 μL PMDETA for 6 min. [2] Then the samples were removed from solution, rinsed with an abundance of ultrapure water and methanol successively to remove both unreacted NIPAAm monomer and un-grafted PNIPAAm, and dried under a nitrogen flow. For comparison, PNIPAAm brushes were also grafted from the homogenous SAMs of ATRP initiators without laser ex-

posure under the identical polymerization conditions. These surfaces were characterized using a variety of analysis techniques as reported previously.[2]

1.4 Surface Analysis

1.4.1 X-ray Photoelectron Spectroscopy

The elemental composition of surfaces was determined with a Kratos Analytical Axis Ultra X-ray photoelectron spectrometer (XPS) equipped with a monochromatic Al Kα source. High-resolution scans were acquired with a pass energy of 20 eV and a step size (resolution) of 0.1 eV. Survey scans were acquired with a pass energy of 160 eV and a step size of 1.0 eV. XPS data were analyzed using CASA XPS software. All binding energies were referenced to the main hydrocarbon peak, designated at 285 eV. Curve fitting was performed using a linear peak base and symmetric 30/70 Gaussian–Lorentzian peak structure.

1.4.2 Atomic Force Microscopy

Imaging of nanopatterned initiator layers was carried out on a MFP 3D scanning probe microscope (Asylum Research, Santa Barbara, CA) in a force modulation operation mode. A function generator (SRS DS 345) was synchronized with a lock-in amplifier (Ametk, model 7280) to extract phase and amplitude information.

Contact-mode topographical imaging of nanopatterned PNIPAAm brushes was carried out using a Digital Instruments multimode atomic force microscopy (AFM) with Nanoscope IIIa controller. AFM imaging in aqueous solutions was done using a fluid cell. Imaging at different temperatures was performed using a fluid cell and a temperature controller (TC), in which, the sample was placed over a small resistor. The resistor was connected to an AC power supply using a controllable ammeter device that is in series with a commercial TC device to heat the sample surface in water. Temperature was maintained with an accuracy of 0.1°C using a k-type thermocouple connected between the TC and ultrapure water in the fluid cell.

1.4.3 Contact Angle Goniometry

Static water contact angle measurements were obtained by sessile drop methods using a contact angle goniometer (Rame-Hart Model 100-00) at room temperature. Each of the average contact angle measurements reported were obtained from six sample replicates.

1.4.4 Ellipsometry

The thickness of unpatterned PNIPAAm brushes was measured using an M-88 spectroscopic ellipsometer (J. A. Woollam Co., Inc.). Each of the average thickness value reported was obtained from three sample replicates. Ellipsometric data were fitted for thickness of the polymer brushes using a Cauchy layer model with fixed A_n (1.47) and B_n (0.01) values.[3]

1.5 Adsorption of Proteins and Nanoparticles (NPs)

1.5.1 BSA and BSA-biotin Adsorption

BSA-Fluor and BSA-biotin were dissolved in PBS (137mM sodium chloride, 27mm potassium chloride, 10mM phosphate buffer) (pH 7.4) or HEPES buffer (10 mM HEPES, 0.15 M NaCl and 0.08% azide, pH=7.5), respectively at a concentration of 0.1 mg/mL. Before protein adsorption, the samples were incubated in PBS for 3 h at ~25°C or ~37°C and then transferred to a sterile 24-multiwell plate with each well containing 500 μL of protein solution.

Protein adsorption proceeded for 3 h under static conditions at either 25°C or 37°C. Following adsorption, the surfaces were immediately immersed in fresh protein-free PBS or HEPES buffer for 10 min (three times) to remove loosely adsorbed protein. Then, the surfaces were briefly rinsed with ultrapure water to remove interfering salt upon the surface and dried under a nitrogen stream.

1.5.2 Adsorption of SA and SA-NPs

SA-Fluor and SA-NPs was dissolved/diluted in PBS at a concentration of 0.01 mg/mL. After adsorption of BSA-biotin at 37°C, the nanopatterned PNIPAAm surfaces were first incubated in PBS for 1 h at 25°C or 37°C and then transferred to a 24-multiwell plate each well containing 500 μL SA-Fluor or SA-NPs solution for 10 min. The samples were then rinsed and dried as described above.

In addition, a control experiment was performed in which SA-Fluor or SA-NPs were pre-incubated in a solution of excess biotin (0.1 mg/mL biotin in PBS) to pre-block the biotin binding sites on SA-Fluor (or SA-NPs) before exposure to the sample surfaces. The SA-Fluor (or SA-NPs) pre-blocked with biotin was subsequently introduced to the nanopatterned PNIPAAm surfaces containing BSA-biotin via the same procedure described above.

1.5.3 Adsorption of Biotin-NPs

Biotin-NPs were diluted with PBS to a final concentration of 0.01 mg/mL. After adsorption of BSA-biotin followed by binding with SA at 37°C, the nanopatterned PNIPAAm surfaces were incubated in PBS for 1 h at 25°C or 37°C and then transferred to 24-multiwell plate each well containing 500 μL of Biotin-NPs solution for 10 min. The samples were then rinsed and dried using the same procedure described above.

1.5.4 Fluorescence Microscopy

The adsorption of proteins and NPs was evaluated using fluorescence microscopy (Zeiss Axio Imager2) with a 40X objective and a 488 nm filter. All images used for comparison of fluorescence intensities were obtained using identical exposure times, image contrast and brightness settings. Fluorescence intensity of images was analyzed using Zeiss Axio Vision software. For each sample, 10 images from random areas across the sample surface were captured and analyzed to obtain average fluorescent intensity.

1.5.5 Scanning Electron Microscopy

The adsorbed SA-NPs on nanopatterned surfaces were observed using FEI XL30 scanning electron microscope (SEM) under ultra-high resolution mode. Before characterization, the samples were sputter coated with a thin layer (~4 nm) of gold.

1.6 Cell Culture and Detachment from Nanopatterned PNIPAAm Brushes

NIH-3T3 fibroblast cells were cultured using Dulbecco's modified eagle medium (DMEM) containing 25 mM glucose (Gibco) supplemented with 10% calf serum (Sigma-Aldrich), 50U/mL penicillin (Invitrogen), 50 μg/mL streptomycin (Invitrogen) and 0.25 μg/mL Fungizone® antimycotic (Invitrogen). Before seeding the cells, nanopatterned PNIPAAm surfaces were sterilized in ethanol for 20 minutes, rinsed three times in PBS, incubated with approximately10 μg/mL bovine fibronectin (Invitrogen) in PBS solution for 4 h at 37°C, and rinsed three times in PBS. For the NIH-3T3 cell studies, PBS comprised 1.06 mM KH_2PO_4, 155.17 mM NaCl, 2.97 mM $Na_2HPO_4 \cdot 7H_2O$, pH=7.4, without Ca^{2+} or Mg^{2+}. The sample surfaces were then placed inside wells (9.6 cm^2/well) within a 6-multiwell plate and cells and were seeded at $4.5x10^4$ cells/well and cultured under standard conditions (37°C and 5% CO_2) for 3 days. Before detachment, cell attached to surfaces were gently washed with PBS and incubated with a live/dead membrane integrity stain (Invitrogen) (solutions were pre-warmed to 37°C). For detachment, surfaces containing cells were transferred to PBS at 25°C and incubated for 1 h and then rinsed by pipetting PBS onto the surfaces. Cell images were obtained using fluorescence microscope (Zeiss Axio Imager2) with a 10X objective. The density of adhered cells was quantified according to the number of adhered cells per unit area as determined by ImageJ software (National Institutes of Health; http://rsbweb.nih.gov/ij/; version: 1.43u). For each sample, 6 images from random areas across the sample surface were captured and analyzed to obtain the average and standard deviation.

2. RESULTS

2.1 Surface Properties of Initiator Layer Before and After Laser Exposure

The surface properties of initiator SAM layer before and after UV laser exposure were examined by XPS, ellipsometry and water contact angle measurements (**Fig. S1** and **Table S1**). The decrease in the layer thickness indicated that the initiator layer was rapidly degraded upon exposure to the laser beam. XPS results indicate that after exposure, the bromide peak disappeared and carbon composition decreased, suggesting that the laser not only removed the bromide groups, but also photodegraded the alkyl chains and generated new functional groups, which contact angle analysis indicated are more hydrophilic. The exact composition of the resultant chemical species obtained after UV photodegradation remains unclear.

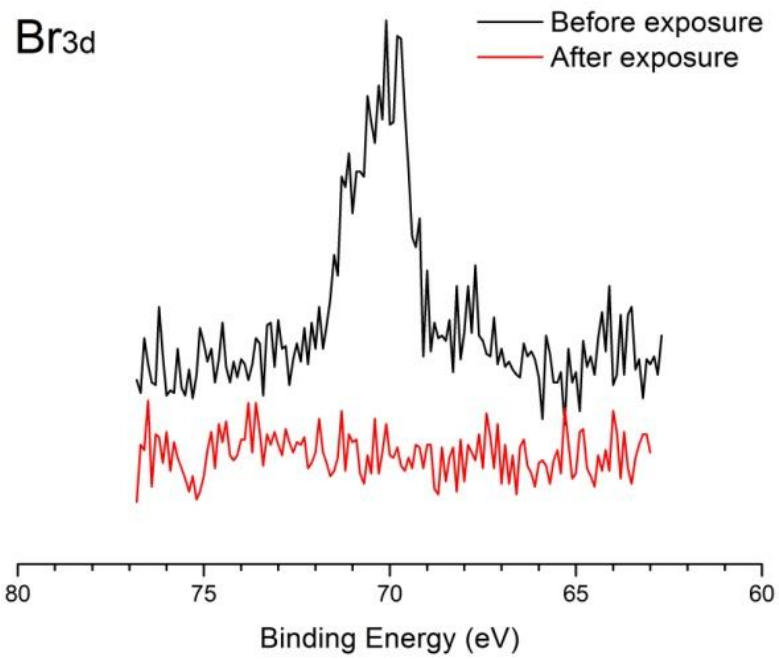

Fig. S1 XPS high-resolution Br_{3d} spectra of initiator layer before and after laser exposure (exposure dose is 13.9 J/cm^2).

Table S1 Elemental composition, thickness and water contact angle of initiator layer before and after laser exposure (exposure dose is 13.9 J/cm^2). Data for thickness and contact angles are means ± the standard error (n=6).

Properties	Chemical composition					Layer thickness (nm)	Contact angle (^{o})
	C (%)	O (%)	Si (%)	Br (%)	C/O		
Before exposure	43.5	29.8	24.5	0.4	1.52	0.84±0.03	70±3
After exposure	27.9	38.4	33.7	-	0.72	0.32±0.04	36±2

2.2 AFM of Nanopatterned Initiator Layer

The nanoscale patterning of the initiator SAM layer by UV IL was confirmed by acoustic AFM, which gave better contrast than other AFM modes.[4] A phase image of a nanopatterned initiator SAM layer is shown in **Fig. S2**. The alternating bright and dark contrast parallel patterns corresponds to non-degraded and photodegraded initiator, respectively. The measured pattern period was ~263 nm and is consistent with the theoretical value (266 nm) based on the equation:

$$\text{Period} = \lambda/[2\sin(\theta/2)]$$

where λ is the wavelength of the laser beam and θ is the interfering angle, here λ=266 nm and θ=60°.

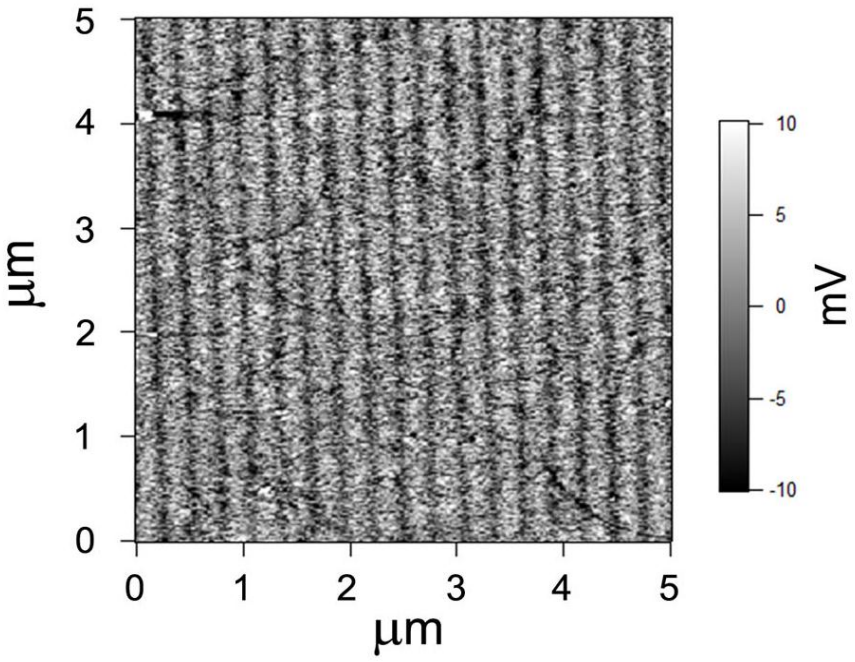

Fig. S2 Acoustic AFM phase image of a nanopatterned initiator SAM layer prepared by UV IL (exposure dose is 13.9 J/cm^2). The image size is 5 x 5 µm and z-contrast range of -10 to 10 mV. The parallel patterns of alternating bright and dark contrasts were observed due to the different chemical properties of the non-degraded and photodegraded initiator.

2.3 Relationships of Height (h) and Extended Width (w) of Nanopatterned Polymer Brushes as a Function of Polymer Stripe Width (Δ)

Based on the simulation results of grafted polymers on nanopatterned surfaces by Patra *et al.*,[6] the dependence of the brush height $h(\Delta, N, \sigma)$ can be expressed as:

$$h(\Delta, N, \sigma) = N\sigma^{1/3}\tilde{h}(\Delta / N) \qquad (1)$$

while the amount by which the brush extends over the edge of the stripe is the excess brush width, w, which can be factorized as:

$$w(\Delta, N, \sigma) = N\sigma^{1/2}\tilde{w}(\Delta / N) \qquad (2)$$

where Δ is the polymer strip width, N is polymer contour length (the polymers are described as freely jointed chains composed of N spherical subunits connected by bonds), σ is grafting density and $\tilde{h}(\Delta / \mathrm{N})$ and $\tilde{w}(\Delta / \mathrm{N})$ are scaling factors.

From equations (1) and (2), it is found that as Δ decreases, (i) the height of polymer brushes also decreases (which has been verified by AFM experimental results previously[7]), and (ii) the extent of polymer lateral extension becomes weaker. Based on these general rules and our AFM images, we have suggested three possible schematic depictions for the distributions for the surface tethered PNIPAAm chains obtained for different IL exposure times (**Fig. S3**).

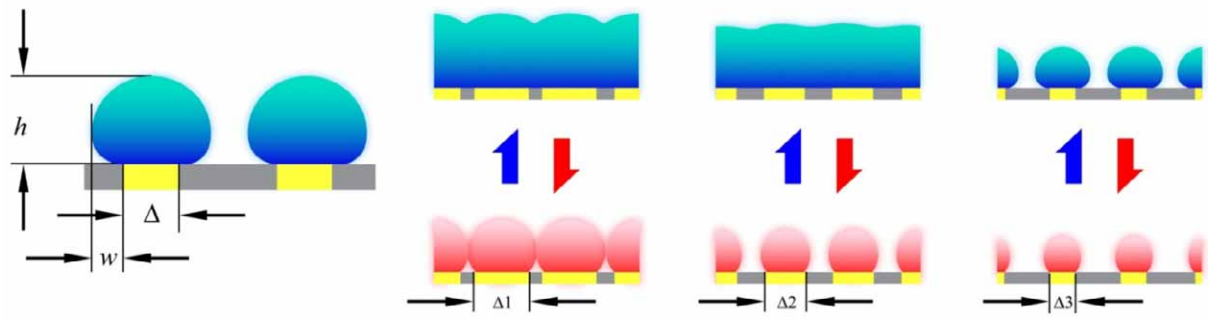

Fig. S3 Schematic representation of contour plots of nanopatterned polymer brushes as prediction from Reference 8.

2.4 BSA-Fluor Adsorption on Control Samples

BSA-Fluor adsorption on unpatterned PNIPAAm and other control surfaces under identical conditions are summarized in **Fig. S4** and **Table S2**. We found that (1) all the tested control surfaces show no significant thermo-responsive protein adsorption behavior ($\Gamma_{37/25}$ value is lower than 1.50); (2) only a slight increase in protein adsorption occurs on unpatterned PNIPAAm surface ($\Gamma_{37/25}$ value of 1.13) indicating negligible thermo-responsivity of the unpatterned polymer;[9] and (3) BSA adsorption on unpatterned PNIPAAm surface is much lower than adsorption on nanopatterned PNIPAAm surface, which is consistent with the protein resistant property of PNIPAAm.[9] Taken together, the results support the hypothesis that most protein adsorbed on the polymer-free intervals (primary adsorption) instead of on, or in, the PNIPAAm brushes themselves. Furthermore, thermo-responsive protein adsorption on nanopatterned PNIPAAm surfaces is due to the conformational changes of PNIPAAm, which controlled (i.e., blocked or facilitated) the access of the protein to the polymer-free substrate.

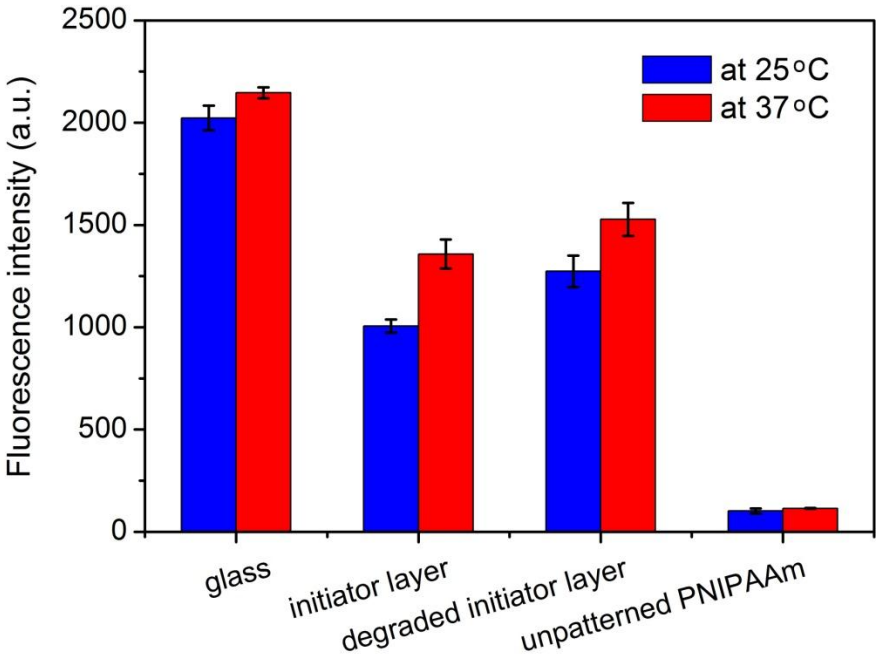

Fig. S4 Comparison of BSA-Fluor adsorption on control surfaces after 3-h immersion in 0.1 mg/mL BSA-Fluor PBS solution at 25°C and 37°C; error bars represent the standard deviation of the mean (n=10).

Table S2 Comparison of BSA adsorption on different surfaces at 37°C and 25°C.

Sample surface	$\Gamma_{37/25}$ value
Unmodified glass	1.06±0.05
Initiator layer	1.35±0.10
Photodegraded initiator layer	1.20±0.05
Unpatterned PNIPAAm surface	1.13±0.11
Nanopatterned PNIPAAm surface	2.10±0.19

BSA-Fluor adsorption at different temperatures and incubation times is summarized in **Fig. S5**. We observed that at 25°C, as the incubation time is increased from 3 h to 24 h, BSA adsorption on nanopatterned PNIPAAm surfaces increases only slightly compared with the level of adsorption measured at 37°C. This result suggests that the swollen nanopatterned PNIPAAm chains at 25°C can exhibit significant shielding toward primary protein adsorption over periods of time much longer than 3 h.

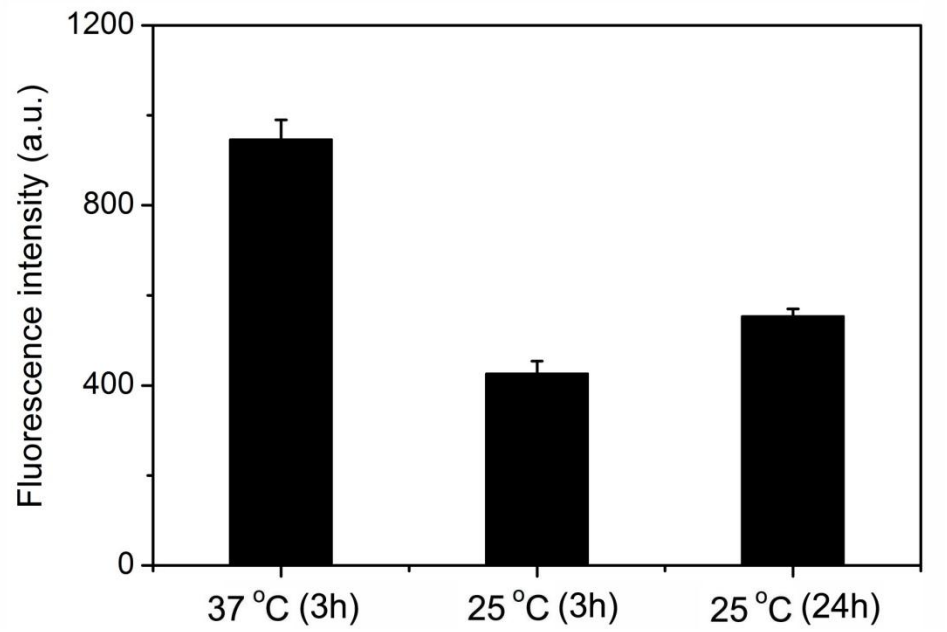

Fig. S5 Comparison of BSA-Fluor adsorption (0.1 mg/mL BSA-Fluor PBS solution) on nanopatterned PNIPAAm surfaces after 3-h immersion at 37°C, 3-h immersion at 25°C, and 24-h immersion at 25°C; error bars represent the standard deviation of the mean (n=10).

2.5 SA-Fluor Adsorption on Control Samples

The levels of SA-Fluor on unpatterned PNIPAAm and other control surfaces under identical conditions are summarized in **Fig. S6** and **Table S3.** These results show that (1) unpatterned PNIPAAm surface without prior adsorption of BSA-biotin exhibit the lowest level of SA-Fluor, which is consistent with protein resistance property of PNIPAAm;[9] (2) SA-Fluor is present in higher quantities on nanopatterned PNIPAAm surfaces pre-treated with BSA-biotin as compared to nanopatterned PNIPAAm surfaces without biotin-BSA pre-treatment. Taken together, these results indicate that the SA-Fluor present on nanopatterned PNIPAAm surfaces with pre-adsorption of BSA-biotin results from the specific binding affinity between SA-Fluor and BSA-biotin.

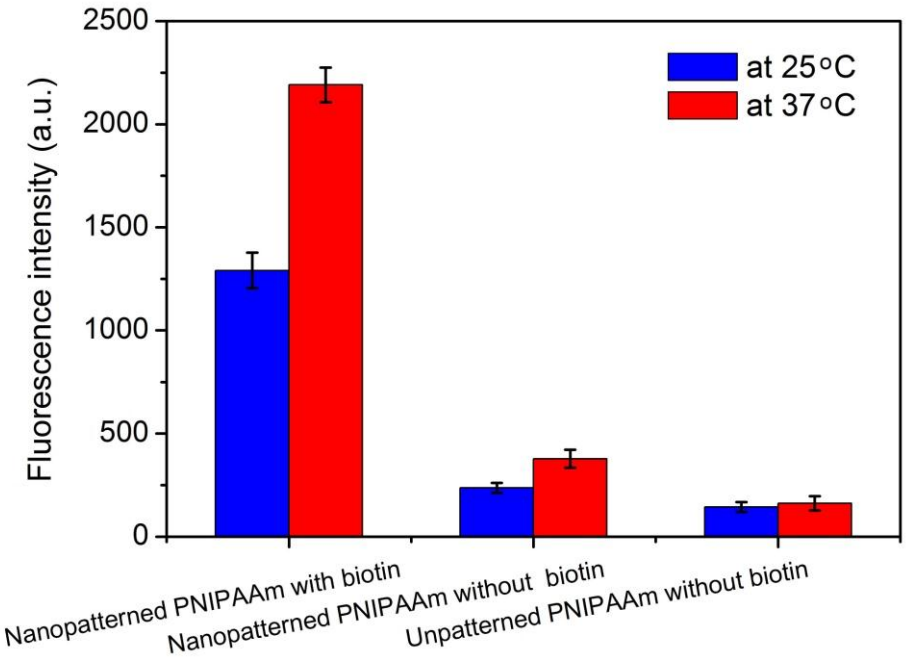

Fig. S6 Comparison of SA-Fluor adsorption on surfaces after 10-min immersion in 0.01 mg/mL SA-Fluor PBS solution at 25°C and 37°C; error bars represent the standard deviation of the mean (n=10).

Table S3 Thermo-responsivity of SA adsorption on different surfaces

Sample surface	$\Gamma_{37/25}$ value
Nanopatterned PNIPAAm surface after adsorption BSA-biotin	1.70±0.15
Nanopatterned PNIPAAm surface without adsorption of BSA-biotin	1.61±0.18
Unpatterned PNIPAAm surface without adsorption of BSA-biotin	1.12±0.12

2.6 SA-Fluor and SA-NPs Adsorption on Nanopatterned PNIPAAm Surfaces with and without Pre-blocking with Biotin

To further verify that adsorption of SA-Fluor and SA-NPs on nanopatterned PNIPAAm surfaces pre-treated with BSA-biotin was biospecific, another control experiment was conducted. SA-Fluor and SA-NPs were pre-incubated in a solution with excess biotin to pre-block all biotin binding sites on the SA-Fluor (or SA-NPs) before adsorption onto the nanopatterned surfaces. As shown in **Fig. S7** it was found that the fluorescence values (corresponding to presence of SA-Fluor or SA-NPs) are much lower if the biotin-binding sites were pre-blocked. This result strongly suggests that the presence of SA-Fluor (or SA-NPs) on nanopatterned PNIPAAm surfaces pre-treated with BSA-biotin is mainly due to the bio-specificity between SA and biotin rather than non-specific adsorption.

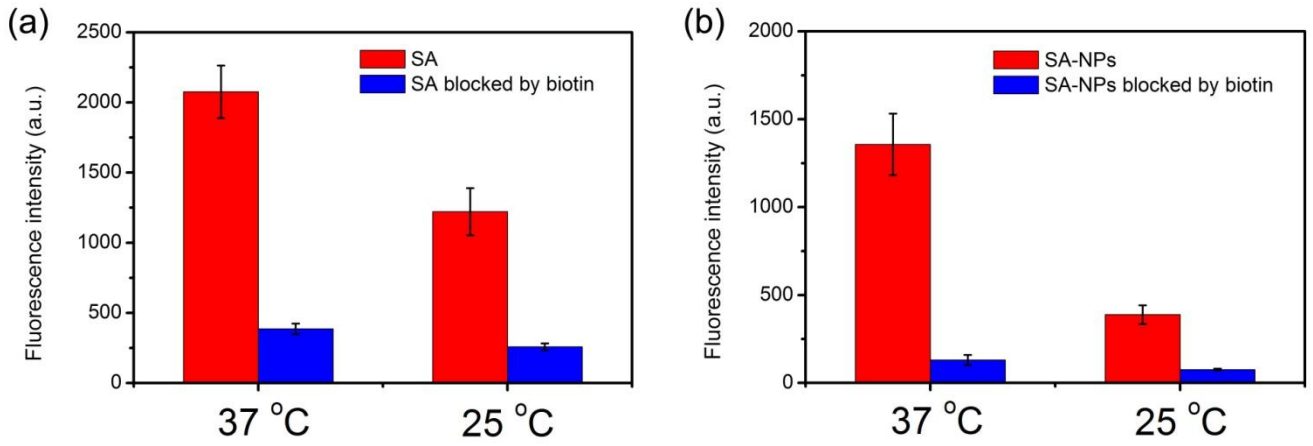

Fig. S7 Comparison of adsorption of (a) SA-Fluor and (b) SA-NP (with and without pre-blocking with biotin) to nanopatterned PNIPAAm surfaces after immobilization of BSA-biotin at 37°C. The concentration of SA-Fluor and SA-NP is 0.01 mg/mL and the adsorption time is 10 min; error bars represent the standard deviation of the mean (n=10).

2.7 Biotin-NPs Immobilization on Micro-and Nanopatterned PNIPAAm Surfaces

To further test thermo-responsive bio-recognition, we employed SA as a bridge between surface-adsorbed BSA-biotin and biotin conjugated fluorescent nanoparticles (Biotin-NPs, d=40 nm). As shown in **Fig. S8** it was observed that for the areas with nanopatterned PNIPAAm brushes, the fluorescence intensity is much lower at 25°C than at 37°C (with a $\Gamma_{37/25}$ value of 3.40±0.27) again demonstrating the ability to control SA exposure via conformation changes of PNIPAAm. Since the biotin-SA system is well established and abundant among commercialized products (e.g. biotinylated antibodies), we anticipated that this model surface holds potential for diverse application in many fields.

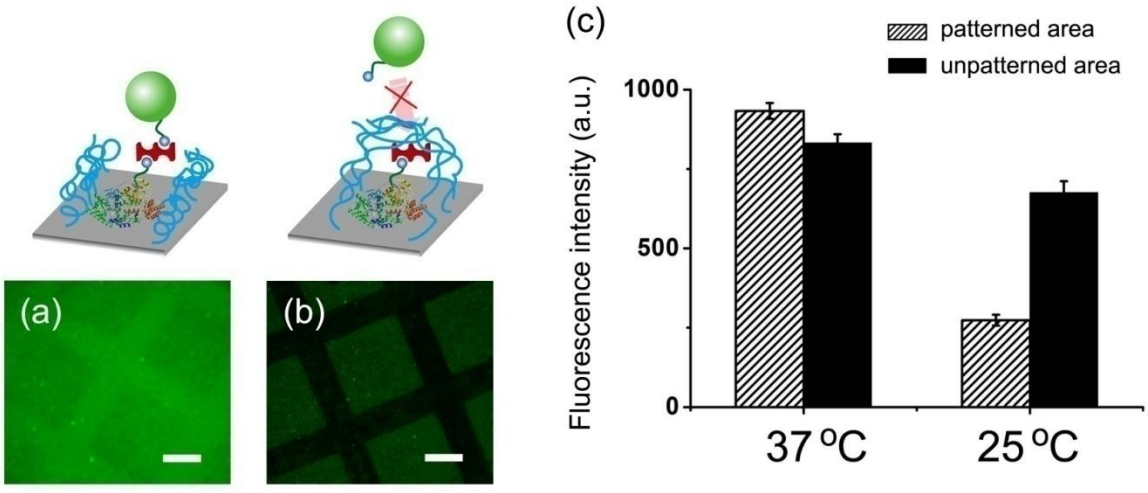

Fig. S8 Fluorescence images of Biotin-NPs on sample surfaces (after immobilization of BSA-biotin followed by SA) at (a) 37°C and (b) 25°C (the concentration of Biotin-NPs is 0.01 mg/mL and the time allotted for binding is 10 min). The square regions are the areas without PNIPAAm brushes and the grid regions are the areas with nanopatterned PNIPAAm brushes. The scale bar in images represents 50 μm. The corresponding fluorescence intensities of nanopatterned area and un-nanopatterned area are indicated in (c). The absolute value of fluorescence intensity shown in data image is the average value based on several section analyses from the fluorescence microscope image using Zeiss AxioVision software. Error bars represent the standard deviation of the mean (n=10). The $\Gamma_{37/25}$ values of patterned area and unpatterned area are 3.40±0.27 and 1.23±0.09, respectively.

3. References

1. J. Adams, G. Tizazu, S. Janusz, S. R. Brueck, G. P. Lopez and G. J. Leggett, *Langmuir*, 2010, **26**, 13600-13606.

2. P. Shivapooja, L. K. Ista, H. E. Canavan and G. P. Lopez, *Biointerphases*, 2012, **7**, 32.

3. K. N. Plunkett, X. Zhu, J. S. Moore and D. E. Leckband, *Langmuir*, 2006, **22**, 4259-4266.

4. J. Zhang, Z. Parlak, C. M. Bowers, T. Oas and S. Zauscher, *Beilstein J. Nanotechn.*, 2012, **3**, 464-474.

5. G. Tizazu, O. El-Zubir, S. R. Brueck, D. G. Lidzey, G. J. Leggett and G. P. Lopez, *Nanoscale*, 2011, **3**, 2511-2516.

6. M. Patra and P. Linse, *Nano Lett.*, 2006, **6**, 133-137.

7. W. K. Lee, M. Patra, P. Linse and S. Zauscher, *Small*, 2007, **3**, 63-66.

8. A. G. Koutsioubas and A. G. Vanakaras, *Langmuir*, 2008, **24**, 13717-13722.

9. Q. Yu, Y. Zhang, H. Chen, Z. Wu, H. Huang and C. Cheng, *Colloids Surf., B*, 2010, **76**, 468-474.